Ground-state properties of LiV_2O_4 and $Li_{1-x}Zn_x(V_{1-y}Ti_y)_2O_4$

M. Brando[1,a], N. Büttgen[1], V. Fritsch[1], J. Hemberger[1], H. Kaps[1], H.-A. Krug von Nidda[1], M. Nicklas[1], K. Pucher[1], W. Trinkl[1], A. Loidl[1], E.W. Scheidt[2], M. Klemm[3], and S. Horn[3]

[1] Experimentalphysik V, Elektronische Korrelationen und Magnetismus, Institut für Physik, Universität Augsburg, 86135 Augsburg, Germany
[2] Experimentalphysik III, Institut für Physik, Universität Augsburg, 86135 Augsburg, Germany
[3] Experimentalphysik II, Institut für Physik, Universität Augsburg, 86135 Augsburg, Germany

Abstract. We present susceptibility, microwave resistivity, NMR and heat-capacity results for $Li_{1-x}Zn_x(V_{1-y}Ti_y)_2O_4$ with $0 \leq x \leq 0.3$ and $0 \leq y \leq 0.3$. For all doping levels the susceptibility curves can be fitted with a Curie-Weiss law. The paramagnetic Curie-Weiss temperatures remain negative with an average value close to that of the pure compound $\Theta \approx -36$ K. Spin-glass anomalies are observed in the susceptibility, heat-capacity and NMR measurements for both type of dopants. From the temperature dependence of the spin-lattice relaxation rate we found critical-dynamic behavior in the Zn doped compounds at the freezing temperatures. For the Ti-doped samples two successive freezing transitions into disordered low-temperature states can be detected. The temperature dependence of the heat capacity for Zn-doped compounds does not resemble that of canonical spin glasses and only a small fraction of the total vanadium entropy is frozen at the spin-glass transitions. For pure LiV_2O_4 the spin-glass transition is completely suppressed. The temperature dependence of the heat capacity for LiV_2O_4 can be described using a nuclear Schottky contribution and the non-Fermi liquid model, appropriate for a system close to a spin-glass quantum critical point. Finally an $(x/y, T)$-phase diagram for the low-doping regime is presented.

PACS. 75.50.Lk Spin glasses and other random magnets – 71.27.+a Strongly correlated electron systems; heavy fermions – 71.10.Hf Non-Fermi-liquid ground states, electron phase diagrams and phase transitions in model systems

1 Introduction

LiV_2O_4 is one of the rare examples of metallic spinels. It crystallizes in the cubic spinel-type structure AB_2O_4, in which the transition metal cations B are surrounded by regular octahedrons of oxygen ions and form a sublattice of corner-sharing tetrahedra. Therefore, considering antiferromagnetic couplings between nearest neighbors, their magnetic moments should be highly frustrated. Measurements of the electrical resistivity have been reported on single-crystalline material more than thirty years ago by Rogers *et al.* [1] and later on by Urano *et al.* [2], characterizing LiV_2O_4 as a correlated metal. The other metallic transition-metal spinels are $LiTi_2O_4$, which is a BCS-type superconductor with a transition temperature as high as $\sim$13 K [3], and magnetite which reveals charge order below the time-honoured Verwey transition [4].

LiV_2O_4 ($d^{1.5}$) and $LiTi_2O_4$ ($d^{0.5}$) are characterized by nominally broken valence states and the former compound, because of narrow d-bands, was thought to be close to charge order. Instead, based on heat-capacity,

susceptibility and NMR results, heavy-fermion behavior has been detected in LiV_2O_4: In particular it shows a high Sommerfeld coefficient of the heat capacity $\gamma(1K) \approx 420$ mJ/mol K², an almost temperature-independent magnetic susceptibility at low temperatures and an anomalous Korringa behavior of the spin-lattice relaxation rate below 10 K [5]. These results have been corroborated by X-ray diffraction [6] and quasielastic neutron scattering [7]. Theoretical arguments have been put forth, how Kondo-compensated heavy fermions may be formed in a transition metal with only one type of d electrons: Localization of one of the vanadium e_g electrons and a band character of the remaining 0.5 electrons/V could qualitatively generate a Kondo-type compensation, characteristic of the f compounds [8,9]. Like most of heavy-fermion systems LiV_2O_4 should be close to magnetic order and spin fluctuations play an important role, but no static magnetic order was observed above 20 mK [5]. It is worth mentioning that the anomalous temperature dependence of the dynamic susceptibility as measured *via* the spin-lattice relaxation in NMR experiments was interpreted by spin fluctuations in an almost ferromagnetic metal [10,11].

[a] e-mail: `manuel.brando@physik.uni-augsburg.de`

An anomalous spectrum of low lying magnetic excitations have also been reported from quasielastic neutron scattering experiments, pointing towards a transition from ferromagnetic spin fluctuations at high temperatures to antiferromagnetic fluctuations below approximately 50 K [7,12]. The nature of this transition is unclear at present.

However, instead of considering a Kondo-type mechanisms, there exists certainly a further possibility to explain the unusual ground-state properties of LiV_2O_4: Due to the geometrical frustration and despite a relatively strong magnetic interaction (the Curie-Weiss temperature is of the order of -36 K), no long range order can be established and a spin-liquid state exists down to the lowest temperatures. If this is true, LiV_2O_4 belongs to those rare examples of spin systems on corner-sharing tetrahedra which remain true spin liquids neither undergoing a spin-glass nor a spin-ice transition [13]. The most prominent spin liquids up to date are Y:ScMn$_2$ and the pyrochlore system $Tb_2Ti_2O_7$ [14]. It is well known that typical spin-liquids reveal similar dynamic susceptibilities when compared to heavy-fermion systems and also show strongly enhanced Sommerfeld coefficients [15]. This is best documented for YMn$_2$ doped with Sc, with a γ coefficient as high as 160 mJ/mol K^2 [16].

Concerning the ground-state properties of spin-liquids detailed model calculations have been performed by Villain [17]. Specifically for cubic B-type spinels he proposed a "cooperative paramagnetic" ground state, with the spins of each tetrahedron forming antiparallel pairs. Exotic spin-glass behavior evolves on doping nonmagnetic impurities at the B-sites or magnetic impurities at the A-sites [17]. Very recently the ground state properties of spin-1 antiferromagnets on corner-sharing tetrahedra have been calculated by Yamashita et al. [18].

In order to resolve this open questions concerning the ground-state properties of LiV_2O_4 and the evolution of spin-glass behavior on doping, we performed a series of experiments on Ti and Zn doped compounds. When substituting Zn for Li, disordered magnetism is induced. An approximate phase diagram of the $Li_{1-x}Zn_xV_2O_4$ system has been determined by Ueda et al. [19], revealing a spin-glass state extending up to Zn concentrations as high as $x = 0.8$. For high Zn doping, a kind of short-range (cluster-like) order occurs, which coexists with the spin-glass state. To our knowledge no systematic studies have been performed for Ti doped compounds. Here we focus especially on low Zn and Ti doping levels close to the pure compound.

2 Experimental details

2.1 Sample preparation and characterization

Polycrystalline LiV_2O_4 was prepared by sintering a mixture of powders of LiVO$_3$ and VO. By sintering powders of VO with xZnO and $(1-x)$LiVO$_3$ we obtained the series $Li_{1-x}Zn_xV_2O_4$ and by mixing LiVO$_3$ with yTiO and $(1-y)$VO we obtained $Li(V_{1-y}Ti_y)_2O_4$, where x and y are the respective concentrations. A slight excess of LiV_2O_3 was added in order to compensate for Li evaporation. Platinum crucibles were used for reaction of the powders at 750 °C for 10 days. The lattice constants were determined by X-ray diffraction and all compounds revealed the pure fcc spinel structure (space group Fd3m). In the pure compound the lattice constant was determined as $a = 0.8253(3)$ nm. Both alloys series show a linear increase of the lattice constant on increasing doping, reaching values of the lattice constant $a = 0.8324(2)$ nm for $x = 0.3$ and $a = 0.8294(6)$ nm for $y = 0.3$. No impurity phases could be detected in the diffraction experiments. From Rietveld refinement we can exclude a statistical distribution of Li and V on A and B sites, respectively. However, we found a rather significant anomaly in the temperature dependence of the susceptibility in the pure compound close to 240 K. In the literature this anomaly usually is connected with the impurity phase V_4O_7, but there also exists an interpretation in terms of a structural phase transition [20]. In order to exclude the latter possibility we performed an X-ray diffraction study between 200 K and 300 K to search for an anomaly in the lattice constant. With decreasing temperature we found a continuous decrease of the lattice constant yielding a thermal expansion coefficient of $\alpha = 6.5 \times 10^{-5}$ K^{-1} and no sign of a structural phase transition. We conclude, that the anomalies detected in the SQUID measurements point towards the existence of V_4O_7 impurity phases in the pure compound. The same series of samples was also investigated in recent NMR [21] and neutron-scattering experiments [7,12].

The dc magnetization measurements were carried out using a commercial SQUID-magnetometer from Quantum Design for fields up to 50 kOe and for temperatures $1.8 < T < 400$ K. The ac susceptibility was determined with the respective options of the same device. For higher fields up to 160 kOe an extraction magnetometer (Oxford Instruments) was employed.

The complex microwave conductivity was measured utilizing the cavity perturbation technique in the temperature range $5 < T < 300$ K. EPR measurements were performed with a Bruker ELEXSYS-E500 spectrometer working at $\nu = 7.2$ GHz in the temperature range $1.5 < T < 300$ K. For cooling a continuous-flow helium cryostat Oxford Instruments was used for $T > 4.2$ K and a cold-finger bath cryostat below liquid-helium temperatures. The magnetic field was controlled by a temperature stabilized Hall probe (Bruker).

NMR measurements were carried out with a phase-coherent pulse spectrometer in the temperature range $1.5 < T < 120$ K. ^{7}Li spectra were collected by the field-sweep method and were fitted to a Lorentzian-line. The center field was irradiated for the spin-lattice relaxation experiment. The spin-lattice relaxation rate $1/T_1$ was determined by an inversion recovery with a $\pi/2 - \tau_D - \pi$ spin-echo sequence. The recovery of the magnetization was fitted using a Kohlrausch function, $M(\tau) = A \exp[-(\tau/T_1)^z]$, with a stretching exponent z to obtain the spin-lattice relaxation T_1 [21].
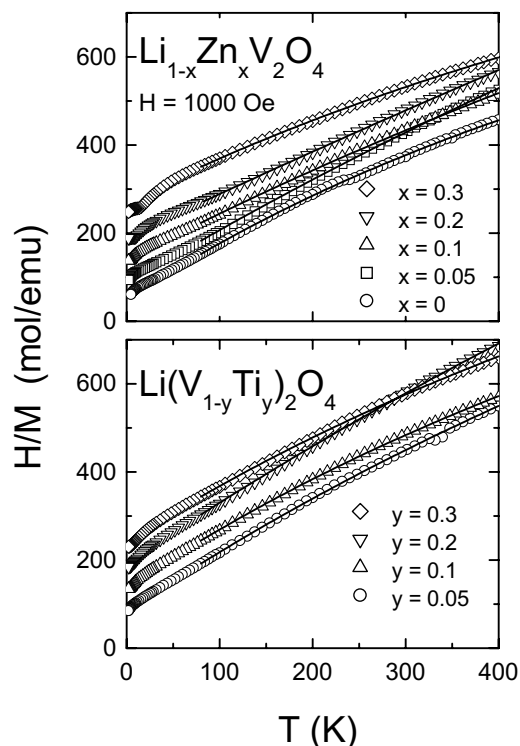
Fig. 1. H/M *vs.* T measured in a static external field of 1000 Oe between $1.5 < T < 400$ K. For clarity, the curves have been offset by 50 mol/emu.

Table 1. Effective paramagnetic moment μ_{eff} per V ion and Curie-Weiss temperature θ for all compounds of the $\mathrm{Li}_{1-x}\mathrm{Zn}_x\mathrm{V}_2\mathrm{O}_4$ and $\mathrm{Li}(\mathrm{V}_{1-y}\mathrm{Ti}_y)_2\mathrm{O}_4$ systems investigated. In fitting $\chi = \chi_0 + C/(T - \theta)$, the diamagnetic and the Van Vleck paramagnetic contributions were held constant at $\chi_0 = 6 \times 10^{-4}$ emu/mol.

x	μ_{eff} per V atom (μ_{B})	θ (K)
0	1.66	−36.6
0.05	1.58	−8.7
0.1	1.75	−21.3
0.2	1.76	−18.2
0.3	1.88	−67.6
y		
0.05	1.48	−36.8
0.1	1.55	−50.8
0.2	1.40	−31.0
0.3	1.58	−55.7

The temperature-dependent specific heat was measured with a standard quasiadiabatic method in an Oxford Instruments ^{4}He cryostat for temperatures $4.2 < T < 50$ K and in an ^{3}He cryostat for temperatures $0.3 < T < 5$ K. The measurements from 2.5 K down to the lowest temperature of about 80 mK were performed using the relaxation method in a ^{3}He/^{4}He dilution refrigerator: In this case the polycrystalline powder was pressed into thin pellets to reduce the τ_2-effect due to the low thermal conductivity of the samples at low temperatures. The specific-heat curves, measured in different temperature ranges, overlap within experimental uncertainties.

3 Experimental results

3.1 Susceptibility and magnetization

The inverse magnetization for all samples investigated is shown in Figure 1. Here we plotted H/M *vs.* T as measured in a static external field of 1000 Oe between $1.5 < T < 400$ K. For better clarity the inverse susceptibilities are shifted by 50 mol/emu with respect to each other, starting with $x = y = 0$. All curves roughly reveal a Curie-Weiss (CW) behavior above ≈ 100 K, in agreement with previous reports [19]. Below 100 K significant deviations from a CW law appear. The high-temperature data have been parameterized assuming the sum of a temperature independent term χ_0, representing Van Vleck and

diamagnetic contributions, and a Curie-Weiss term (solids lines in Fig. 1). For all compounds the data have been fitted in the temperature interval $100 < T < 400$ K. The fits of the high-temperature susceptibility data give approximately the same result for $\chi_0 \approx 6 \times 10^{-4}$ emu/mol in every compound. Then, we kept this value constant and performed the fits again. The parameters of the best fit, the Curie-Weiss temperature θ and the effective paramagnetic moment μ_{eff} per V atom are shown in Table 1. μ_{eff} slightly increases with increasing Zn doping, but remains quite constant for $0 \leq y \leq 0.3$. Concerning the pure compound and using oversimplified arguments based on localized moments, one expects a mixture of $S = 1/2$ and $S = 1$ vanadium ions with an effective paramagnetic moment of about $2.34\mu_{\mathrm{B}}$, which is larger than the observed value. The observed value of $1.66\mu_{\mathrm{B}}$ for $\mathrm{LiV}_2\mathrm{O}_4$ is close to that expected for a $S = 1/2$ momentum/V as observed by Kondo *et al.* and by Urano *et al.* [5,2]. The Curie-Weiss temperature θ remains negative for all samples, indicating an antiferromagnetic coupling between the magnetic moments even at high temperatures. The Θ values reveal a relatively large scatter between −9 K and −68 K, with no specific trend as function of concentration. This probably is due to the fact that we left χ_0 constant and only used an extrapolation of the high temperature susceptibility values to determine Θ. Probably the Van Vleck contributions reveal slight temperature dependence which again increases the error of the CW temperature. The Θ values yield an average value of about −36 K close to that of earlier reports for the pure compound [5,22]. It is worthwhile to mention that a detailed analysis of the susceptibilities and heat capacities of a number of pure samples have been systematically investigated by Johnston and coworkers [22,23].

For temperatures below 25 K the dc susceptibility M/H, measured at 1 kOe, is shown in Figure 2 for all compounds. For Zn doping, already at $x = 0.05$ a cusp-like anomaly can be detected close to $T = 3$ K. This anomaly shifts to higher temperatures on increasing Zn concentration x. Similar anomalies appear in the Ti-doped
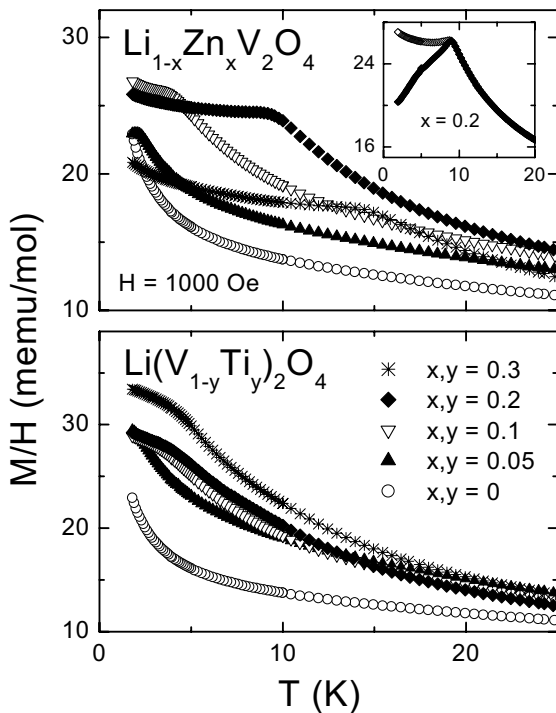
Fig. 2. Low temperature magnetization M/H in a static external field of 1000 Oe. The inset shows the ZFC and FC ($H = 50$ Oe) magnetization curves for $x = 0.2$, indicating the spin-glass freezing temperature T_{f} [24].

Fig. 3. Field-cooled and zero-field-cooled measurements on Li(V$_{1-y}$Ti$_y$)$_2$O$_4$ for $y = 0.05$, 0.1 and 0.2.

Fig. 4. Microwave conductivity σ, normalized to the 300 K, plotted on a logarithmic scale *vs.* temperature between $4.2 < T < 300$ K. In the inset the low-temperature data are shown on a linear scale for $x \leq 0.3$.

compounds, however they appear to be much more smeared out. At the temperature of the anomaly of the dc magnetization, the field-cooled (FC) and zero-field cooled (ZFC) curves split, which characterizes the appearance of a low-temperature spin-glass state. Hence, these anomalies were interpreted as spin-glass freezing temperatures. As an example the FC and ZFC magnetization measurements for $x = 0.2$ are displayed in the inset of Figure 2. A detailed investigation of the spin-glass behavior of Li:ZnV$_2$O$_4$ has been published by Trinkl *et al.* [24]. Field-cooled and zero-field-cooled results for Li(V$_{1-y}$Ti$_y$)$_2$O$_4$ are shown in Figure 3.

For $y = 0.1$ and $y = 0.2$ a clear splitting of FC and ZFC curves is observed. The splitting gives a rough measure of the spin-glass freezing temperature T_{f}. Astonishingly, for $y = 0.1$ and $y = 0.2$ the freezing temperature remains constant at $T_{\mathrm{f}} \approx 4$ K. An additional minor splitting of the two branches can be observed at temperatures close to 9 K for $y = 0.2$ and close the spin-glass anomaly at about 4 K for $y = 0.1$. Such a behavior was already observed in Li$_{1-x}$Zn$_x$V$_2$O$_4$ for $x \geq 0.8$ by Ueda *et al.* [19], although in the Ti-doped samples this effect is certainly weaker. Ueda *et al.* interpreted this effect as the onset of cluster formation. But these anomalies could indicate that freezing phenomena set in already significantly above T_{f}. More investigations are needed to clarify the origin of this transition. The significant differences in the spin-glass dynamics of the Zn and Ti doped compounds may hint towards the fact that in the first case the A-site of the spinel lattice
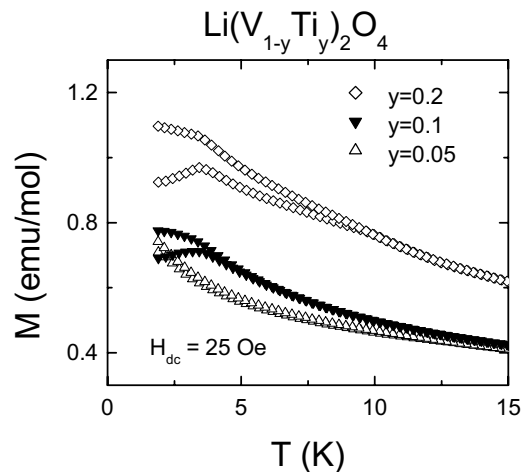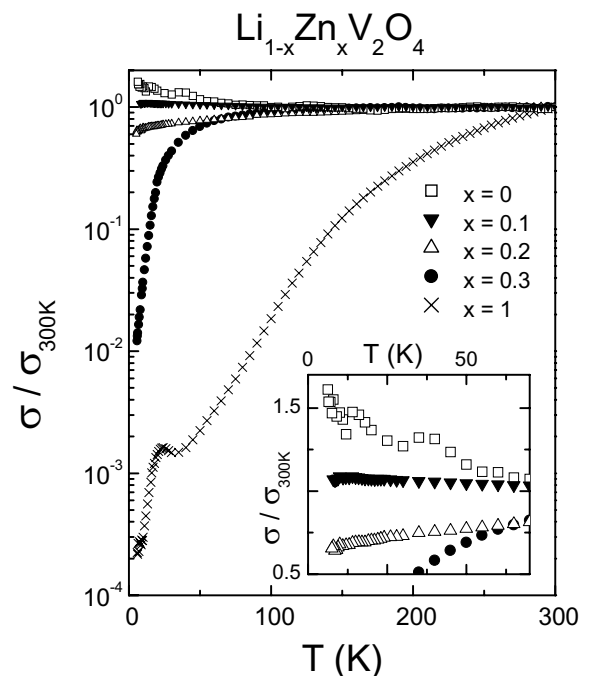
is doped leaving the spin system undiluted. In the second case vanadium is replaced by titanium, strongly disturbing the B-site spins and probably relaxing the magnetic frustration.

3.2 Microwave conductivity

We did not succeed in providing reliable measurements of the dc conductivity in the ceramic samples, even not with high excitation voltages. Contact free measurements of the microwave conductivity for a series of Zn doped compounds including pure ZnV$_2$O$_4$ are shown in Figure 4.

Here the logarithm of the conductivity σ as measured at 7.2 GHz is plotted *versus* the temperature T. The pure Zn compound reveals a purely semiconducting behavior with a strongly decreasing conductivity on decreasing temperature. The anomaly close to 40 K indicates a transition into the antiferromagnetic ground state in a lattice with a tetragonal distortion. From previous work it is known that ZnV_2O_4 reveals a cubic to tetragonal phase transition close to 50 K and subsequently a transition into an antiferromagnetic ground state at 40 K [19]. The compound with $x = 0.3$ still reveals a strongly semiconducting characteristic. From these measurements we conclude that the metal to insulator transition is close to $x = 0.2$ and that the low-doped ceramic samples reveal metallic conductivity for all temperatures below 300 K. The inset of Figure 4 shows the low-temperature conductivity for the samples with $x < 0.3$ on a linear scale. For the pure compound the increase of the conductivity is about a factor of two when cooling from room temperature down to the lowest temperatures. The conductivity has been measured on single crystalline LiV_2O_4 by Rogers *et al.* [1] and recently by Urano *et al.* [2]. In these measurements the resistivity increases by almost a factor of 5, respectively 20, revealing that our polycrystalline material is still dominated by numerous defects and grain boundaries. Previous work on ceramic Li:ZnV_2O_4 showed metallic conductivity only in pure LiV_2O_4 and only at rather high temperatures [25].

3.3 Magnetic resonance

3.3.1 EPR results

Pure LiV_2O_4 is EPR silent and no signal due to a localized V magnetic moment can be observed. However defect states, most probably free V spins located in domain walls and grain boundaries, can be detected. A rough estimate shows that approximately a fraction of 0.2–0.5% of the vanadium ions contributes to the signal which will also contribute to the bulk magnetic susceptibility at low temperatures. Resonance absorption appears at g-values close to 2, which typically is observed in V compounds and represents the spin-only value with a negligible small spin-orbit coupling. In this sense EPR can serve as an experimental method to determine the purity of the samples. However, as is often observed, the defect spins are closely connected to the spin fluctuations which dominate the bulk sample, a situation which is described as a strong bottleneck. In this situation the defect spins directly follow the bulk susceptibility and can serve as a local probe of the magnetic properties. In addition, the defect spins are exposed to local static fields created by the freezing of spins in the local environment. This random fields will be reflected by the line width of the resonance absorption. The temperature dependence of the EPR line width at resonance absorption was measured in pure LiV_2O_4 and in the doped compounds with $x = 0.3$ and $y = 0.3$ [26]. Astonishingly, the line-width broadening, which strongly increases towards low temperatures, is strongest in the

Zn doped compound, but weakest in the Ti doped samples. In agreement with the magnetization measurements, the substitution of Li by Zn induces frozen-in spin configurations while in the Ti doped compounds these static magnetic clusters yield only minor contributions. It is important to note that the temperature dependencies of the inverse intensities of the EPR absorption nicely resemble the Curie-Weiss behavior observed in the bulk susceptibility measurements and demonstrate that the defect spins really experience a strong bottleneck situation. Moreover the line width linearly increases on increasing temperatures beyond 150 K, but this Korringa-like slope is almost a factor of 50 lower than in normal metals [26].

3.3.2 NMR experiments

A detailed NMR study of line width, Knight shift, spin-spin and spin-lattice relaxation rates in pure and doped LiV_2O_4 has been published previously [5,11,21,27,28]. In this work we would like to focus on one important aspect: We study in detail the spin-lattice relaxation rates close to the freezing transition temperatures in Zn and Ti doped compounds. The spin lattice relaxation rate $1/T_1$ is a direct measure of the imaginary part of the dynamic susceptibility and is determined by $1/T_1 \propto T\chi_0/\Gamma(T)$ where χ_0 and Γ denote the static susceptibility and the magnetic relaxation rate, respectively. These are the decisive properties of the electronical environment driving the nuclear relaxation process. In heavy-electron systems $1/T_1$ is a linear function of T with a highly enhanced slope. And indeed, this behavior has been observed in pure LiV_2O_4 by Kondo *et al.* between 1.5 and 5 K [5]. Recently we have published low-temperature spin-lattice relaxation rates down to 30 mK [29,30]. We have found a striking anomaly close to 0.6 K which reveals a strong frequency dependence and has been interpreted as the continuous slowing down of spin fluctuations due to frustration effects [29,30]. At present it is unclear if this anomaly is a reminder of a spin-glass-like transition due to defect states or an indication for a gap-like behavior of the pure compound.

Figure 5 shows the results of the temperature dependence of the spin-lattice relaxation rates in the pure and doped compounds. The results are presented on double-logarithmic scales for Zn concentrations $x = 0$, 0.05, 0.1, 0.15, 0.2 and 0.3 (upper frame of Fig. 5) and for Ti concentrations $y = 0$, 0.025, 0.05, 0.1 and 0.2 (lower frame of Fig. 5). In the Zn compounds, close to the spin-glass transition temperatures, the longitudinal relaxation rates become dramatically enhanced. Compared to observations in canonical spin-glasses, unusual sharp anomalies appear for $x = 0.1$, 0.15 and 0.2. Certainly these anomalies are reminiscent to observations close to magnetic phase transitions. However, from careful susceptibility measurements the spin-glass state has been clearly established [24]. For $x = 0.3$ (inset in the upper frame of Fig. 5) the cusp-shaped maximum is strongly suppressed, but still indicates critical behavior. For $x = 0.05$ a smooth maximum shows up close to 2 K, indicating a smooth slowing down
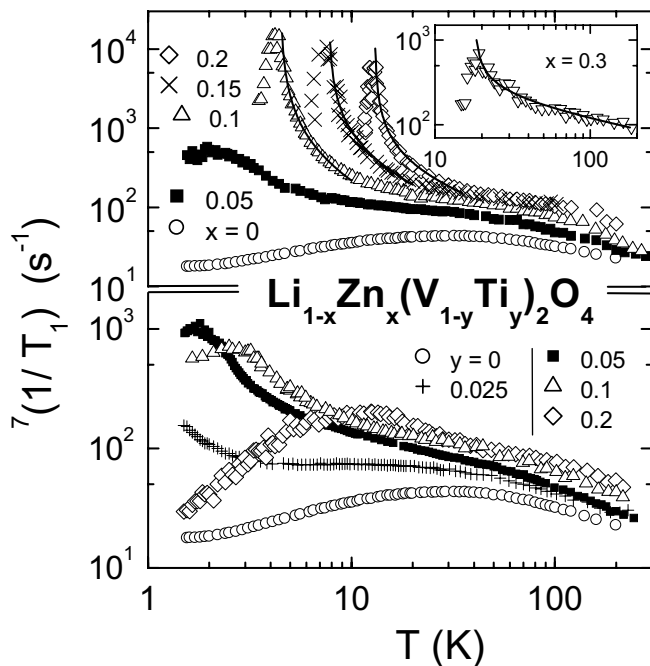
Fig. 5. Temperature dependence of the spin-lattice relaxation rate $1/T_1$ for $\text{Li}_{1-x}\text{Zn}_x(\text{V}_{1-y}\text{Ti}_y)_2\text{O}_4$ for temperatures $1.5 < T < 300$ K in a double logarithmic scale. In the upper panel, the solid lines correspond to fits using the equation $1/T_1 = A(T - T_{\text{crit.}})^{-\delta}$. In the inset the behavior of the sample with $x = 0.3$ is shown.

of the spin degrees of freedom rather than a well defined spin-glass transition. A different behavior is observed for the titanium doped compounds. Here smooth maxima are observed for $y = 0.05$ and 0.1 similar to the observations in $\text{Li}_{0.95}\text{Zn}_{0.05}\text{V}_2\text{O}_4$, but a broad and smeared out maximum is observed in $1/T_1$ *vs.* T for $y = 0.2$. It seems important to note that this broad maximum appears approximately at 10 K and corresponds to the observation of the first splitting of FC and ZFC magnetization (see Fig. 3). However in the magnetization experiments this is a small effect and the cusp like anomaly close to 3 K does not show up in the temperature dependence of the spin-lattice relaxation. On the contrary, for the Zn doped samples the cusp shaped anomalies in $1/T_1(T)$ and the splitting of FC and ZFC magnetization coincide. The splitting appears close to 9 K for $x = 0.2$ (see inset in upper frame of Fig. 2), the sharp anomaly in $1/T_1(T)$ close to 12 K for $x = 0.2$. The observed shift may well be explained assuming the severe differences in the measuring frequencies and by the fact that the spin-lattice relaxation rates have been measured in external fields of about 10 kOe. The differences in the freezing dynamics for Zn and Ti doped compounds can probably be attributed to the increasing metallicity for decreasing x as was been deduced from conductivity measurements above and, in addition, to the increasing metallicity for increasing y as it is indicated by the linear behavior of the temperature dependent spin-lattice relaxation rate $1/T_1(T)$ for the Ti concentration $y = 0.20$ below $T \approx 6$ K. In view of the differences in the freezing dynam-

ics for Zn and Ti doped compounds it is important to note that on Zn doping, the three-dimensional network of V spins is not diluted, but only disturbed *via* local crystal field effects and local lattice distortions, while for Ti doping the frustrated network is directly disturbed.

For the Zn doped compounds we made an attempt to describe the increase of the spin-lattice relaxation rates on approaching the freezing temperatures assuming a critical behavior with $1/T_1 = A(T - T_{\text{crit.}})^{-\delta}$, with δ being a critical exponent and $T_{\text{crit.}}$ characterizing a critical temperature. The results of these fits are indicated as solid lines in the upper frame of Figure 5. For $x = 0.1, 0.15$ and 0.2 we were able to describe consistently $1/T_1(T)$ using an exponent $\delta = 1$. However, for $x = 0.3$ the exponent is considerably smaller, and the fit shown in the inset of Figure 5 has been calculated assuming $\delta = 0.4$.

3.4 Specific heat

In this chapter we report heat-capacity measurements on $\text{Li}_{1-x}\text{Zn}_x(\text{V}_{1-y}\text{Ti}_y)_2\text{O}_4$ system for $x = 0, 0.1$ and 0.3, and $y = 0.3$. The LiV_2O_4 sample was already investigated in NMR, heat-capacity [24,29] and neutron-scattering experiments [7]. Figure 6 shows the heat-capacity results as observed in pure LiV_2O_4 and in the Ti-doped compound with $y = 0.3$ for temperatures $T > 2$ K. Here the data are plotted as C_P/T *vs.* T^2 to indicate the heavy-fermion (HF) behavior. Both compounds reveal a rather enhanced Sommerfeld coefficient γ for temperatures $15 < T < 25$ K, which extrapolates roughly towards 150 mJ/mol K^2. Even this is one of the highest γ values observed in d-metal compounds. At low temperatures both compounds reveal a strong increase towards low temperatures. This increase is strong for the pure compound and C_P/T approaches ≈ 400 mJ/mol K^2 at 2 K in good agreement with published results [5,23]. The increase is much less significant in the Ti-doped compound. In order to investigate the nature of the low-temperature behavior, we tried to fit the C_P/T data with a Fermi-liquid model, using

$$C_\text{P}/T = \gamma + \beta T^2 + \delta T^2 \ln\left(\frac{T}{T^*}\right) \qquad (1)$$

where the first two terms correspond to the T-linear electronic and the T^3 phononic contribution, respectively. The last term in equation (1) is a correction term still within the Fermi-liquid theory [31]. The result of the fit is indicated as a dashed line in Figure 6 and corresponds to the following parameters: $\gamma = 420$ mJ/mol K^2, $\beta = 55 \times 10^{-4}$ J/mol K^4, $\delta = 3$ mJ/mol K^4 and $T^* = 120$ K. It is valid in a limited temperature range only. Figure 7 shows C_P/T *vs.* T on a logarithmic scale for $x = 0, 0.1$ and 0.3. For the pure sample C_P/T follows a linear increase for more than one decade, typical of non-Fermi liquid (NFL) behavior in many HF systems [32–34]. Guided by these observations we tried a fit with the following equation

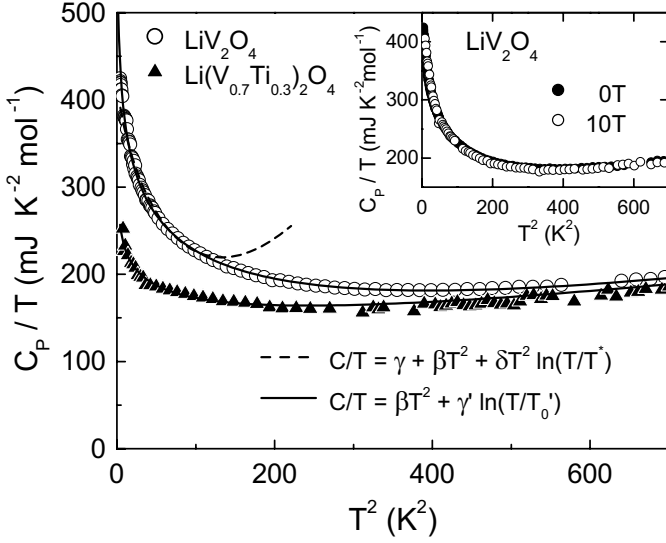$$C_\text{P}/T = \beta T^2 + \gamma' \ln(T'_0/T). \qquad (2)$$

Fig. 6. Specific heat plotted as C_P/T *vs.* T^2 for LiV_2O_4 and the doped sample with $y = 0.3$ for temperatures down to 2 K. The dashed line shows the fit on LiV_2O_4 with the Fermi-liquid model. The solid line corresponds to the behavior expected in the NFL theory and it provides a reasonable approximation of the results. The inset shows a measurement on LiV_2O_4 in zero magnetic field and in 10 tesla [21].

Fig. 7. Specific heat plotted as C_P/T *vs.* $\log T$ in the temperature range 80 mK $< T <$ 50 K for $x = 0$, 0.1 and 0.3. The solid line indicates fits performed using the NFL theory and a Schottky contribution at the lowest temperatures [29]. Literature data for $Li_{4/3}Ti_{5/3}O_4$ from Johnston *et al.* are also shown [23].

Here only a $T\ln(T)$ term is used in addition to the T^3 phonon contribution. This term is characteristic for NFL behavior for systems with a $T = 0$ K magnetic phase transition. In terms of spin fluctuation theories T_0' is a characteristic temperature. Indeed this model function provides an excellent fit for both systems in the complete temperature range (solid line in Fig. 6), yielding a characteristic temperature T_0' of about 47 K and 137 K for the pure and the doped compound, respectively. The Debye temperature Θ_D was derived by the β coefficient in equation (2) with $\Theta_D = (1944r/\beta)^{1/3}$ and $r = 7$, as also calculated by Johnston *et al.* [23]. It results to be 430 K for LiV_2O_4 and 480 K for the doped compound. The fit results for γ' are 144 mJ/mol K^2 and 60 mJ/mol K^2 for $x = y = 0$ and $y = 0.3$, respectively. NFL behavior is expected in systems close to a quantum critical point (QCP), where a magnetic phase transition appears at 0 K [32,33]. We can summarize the observations of Figure 6 with a new interpretation, namely that LiV_2O_4 is a HF system with a Sommerfeld coefficient close to 150 mJ/mol K^2 and with NFL contributions becoming dominant below 15 K. If spin fluctuations are responsible for the enhancement of C_P/T, this seems naturally to characterize LiV_2O_4 as a frustrated magnet with a zero-Kelvin phase transition, which is dominated by strong spin fluctuations at low temperatures.

Before passing to the low-temperature measurements we show heat-capacity measurements in an external field of 10 T. As demonstrated in the inset of Figure 6, the heat capacity remains almost the same in zero field and in a magnetic field of 10 T.
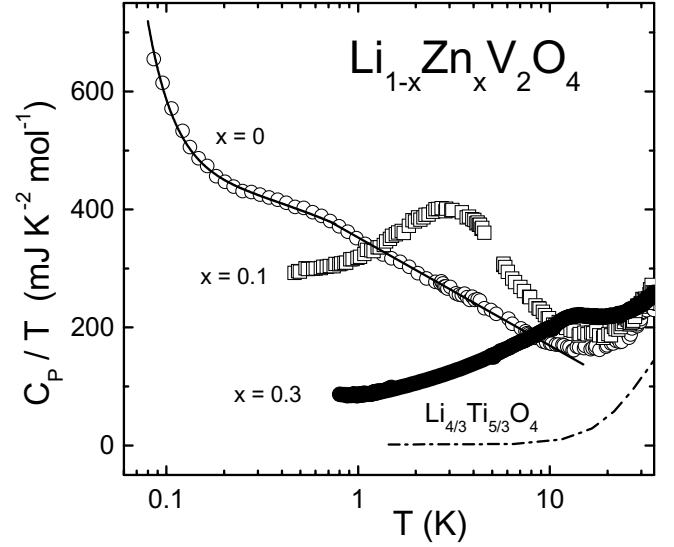
The low-temperature results for LiV_2O_4 are shown in Figure 7. Here the heat-capacity data for temperatures 80 mK $< T <$ 30 K are plotted as C_P/T *vs.* $\log T$. In the same figure the results for $Li_{1-x}Zn_xV_2O_4$ with $x = 0.1$ and 0.3, and for the isostructural non-magnetic insulator $Li_{4/3}Ti_{5/3}O_4$ are also displayed. $Li_{4/3}Ti_{5/3}O_4$ data were taken from Johnston *et al.* [23], and they have been used to estimate the lattice contribution. A logarithmic increase of C_P/T *vs.* $\log T$ for $T \leq 10$ K, a plateau below 1 K and a further sharper increase, due to a Schottky anomaly of nuclear origin, can be observed.

Having subtracted the lattice contribution deduced from the non-magnetic reference compound, a detailed analysis of the electronic heat capacity ΔC_P of LiV_2O_4 can be performed on the basis of the NFL theory and on the high-temperature part of the nuclear Schottky-type specific heat proportional to T^{-2}. The solid line in Figure 7 represents the sum of the best fit performed in the temperature range $80 < T < 600$ mK with

$$C_P/T = \gamma + \frac{\alpha}{T^3} - \eta\sqrt{T} \qquad (3)$$

and the logarithmic-dependent term $T\ln(T)$ between 600 mK $< T <$ 10 K. Here we took the $\sqrt{T}$ term into account, which represents the corrections for a $T \to 0$ K antiferromagnetic [32] or spin-glass transition [35]. We obtained the following fit parameters: $\gamma = 490$ mJ/mol K^2, $\alpha = 0.13$ mJK/mol and $\eta = 137$ mJ/mol K$^{5/2}$. A more detailed analysis is published by Kaps *et al.* [29]. They have calculated $\Delta C_P/T$ utilizing the Moriya's spin-fluctuation theory [32], assuming a system close to an antiferromagnetic instability [36]. The single-impurity

Kondo model can not describe the logarithmic increase of $\Delta C_P/T$ towards low temperatures, while the Moriya's spin-fluctuation theory (with a characteristic temperature $T_0 = 26$ K) roughly agrees with the experimental results, but the extended $\log T$ regime of C_P/T is underestimated [29].

The origin of the low-temperature Schottky contribution is not clear. It indicates that the nuclear-level degeneracies of the ^{7}Li (nuclear spin $I = 3/2$) or the ^{51}V ($I = 7/2$) nuclei are removed due to effective (hyperfine) magnetic fields $B_{\rm eff}$. It cannot be driven by finite electric-field gradients, because the Li and V atoms are located in the A and B sites with crystalline symmetry $T_{\rm d}$ and $O_{\rm h}$ respectively, where the electric-field gradient in the normal spinel structure should be zero. A local distortion at the A sites (Jahn-Teller effect) could lead to an interaction between the electric-field gradient and the electric quadrupole of the Li nuclei, as shown by Hagino et al. [37], but no Jahn-Teller distortion was observed in LiV$_2$O$_4$. Moreover, NMR experiments reveal the absence of any electric-field gradient at the ^{7}Li atoms, and the behavior of the line width suggests that internal magnetic fields are present [29]; they become frozen and remain constant below 1 K. Therefore, the Schottky anomaly should be of magnetic origin and the proportional factor α in equation (3) can be written [38]

$$\alpha = \frac{R}{3} I(I+1) \left(\frac{h\gamma_{\rm NMR}}{k_{\rm B}} \right)^2 B_{\rm eff}^2 \qquad (4)$$

where $\gamma_{\rm NMR} = \nu_{\rm NMR}/B_{\rm eff}$ is the NMR-frequency $\nu_{\rm NMR}$ which gives the energy splitting $h\nu_{\rm NMR}$ in an effective magnetic field $B_{\rm eff}$ of 1T and it can be calculated for every isotope. We made calculations with equation 4 for ^{51}V nuclei, using $\alpha = 0.13$ mJK/mol. An effective magnetic field $B_{\rm eff} = 4.24$ T at the ^{51}V site results: It is small when compared with fields in magnetically ordered systems, which are of the order of some tenths of tesla. We conclude that the Schottky anomaly below 0.2 K arises from frozen-in magnetic effective fields at the ^{51}V nuclei.

In the doped samples a broad maximum is observed at temperatures $T_{\rm g} \approx 3$ K for $x = 0.1$ and ≈ 13 K for $x = 0.3$. Considering the recent works of Ueda et al. [19], Trinkl et al. [24] and Urano et al. [2], these anomalies can be attributed to a spin-glass-like transitions associated with vanadium moments which are antiferromagnetically coupled and geometrically highly frustrated. The characteristic behavior of the specific heat does not resemble that of canonical spin-glasses: e.g. $T_{\rm g}$ does not lie above the freezing temperature $T_{\rm f}$ determined in the ac susceptibility. Moreover, at low T the temperature dependence of ΔC_P is significantly stronger than linear. However in other strongly correlated spin glasses, like URh$_2$Ge$_2$, this dependence varies between T and T^2 as in our case [39].

After having subtracted the lattice contribution taken from Li$_{4/3}$Ti$_{5/3}$O$_4$, we have determined the electronic and magnetic specific heat $\Delta C_P(T)$, which is shown in Figure 8. In all samples strong electronic correlations, indicated by a large value of the Sommerfeld coefficient
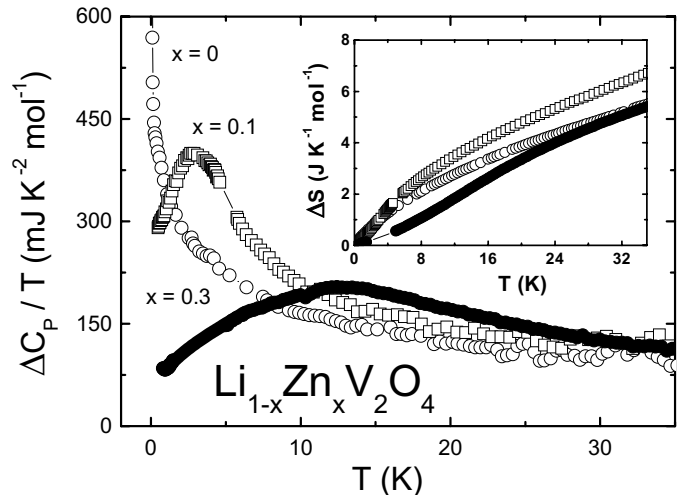

Fig. 8. Electronic and magnetic specific heat ΔC_P for $x = 0$, 0.1 and 0.3 obtained by subtracting the lattice contribution of the isostructural non-magnetic insulator Li$_{4/3}$Ti$_{5/3}$O$_4$ [23]. $\Delta C_P/T$ is plotted vs. T for temperatures 80 mK $< T <$ 35 K. In the inset the temperature-dependent entropy $\Delta S(T)$ is shown.

$\gamma(T) = \Delta C_P(T)/T$, persist up to the high temperatures of about 30 K in agreement with the results obtained by Johnston et al. [23]. With increasing temperature all curves seem to achieve the same value at about 35 K, with $\gamma \approx 125$ mJ/mol K^2. If we approximate $\Delta C_P/T$ with a constant value for $T \to 0$, we can calculate the temperature dependence of the entropy using $\Delta S(T) = \int_0^T \Delta C(T)/T \, {\rm d}T$. The results of the calculations are shown in the inset of Figure 8. Assuming that every vanadium atom contributes with a spin $1/2$, the total entropy released should approach $S_{\rm tot} = 2R \ln 2 = 11.52$ J/mol K for all samples. Looking at ΔS vs. T, as given in the inset of Figure 8, we conclude that only a fraction ($\approx 10\%$) of the spin entropy is lost at the spin-glass transitions. A similar behavior was observed by Urano et al. [2]. Probably not all vanadium atoms take part in the spin-glass freezing process, i.e. below $T_{\rm g}$ they are not all completely frozen. If we speculate that also contributions from the orbital degrees of freedom come into play, Figure 8 documents that also no entropy due to the melting of frozen-in orbital configurations can be detected.

3.5 Discussion and conclusion

Before starting the discussion section it seems interesting to construct an $(x/y, T)$-phase diagram of Li$_{1-x}$Zn$_x$(V$_{1-y}$Ti$_y$)$_2$O$_4$, especially for the region of low doping levels, which have been investigated in the present work. Here we also include the results which have been previously published by our group [21,24]. The spin-glass transitions on Zn doped samples have also been investigated by NMR and susceptibility measurements by
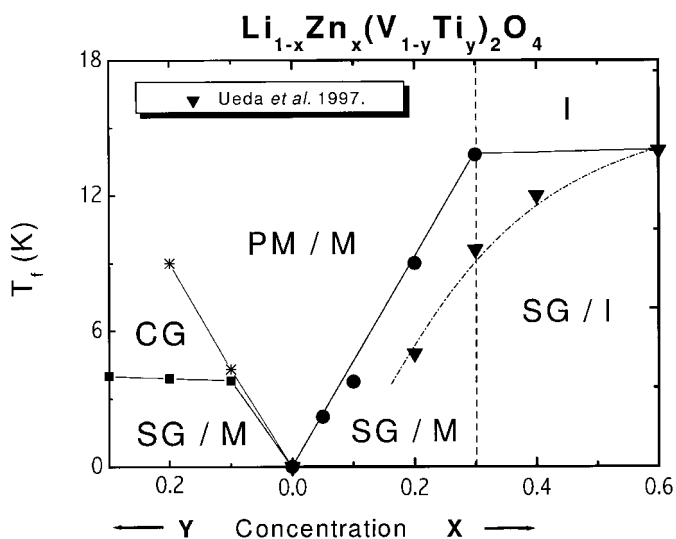
Fig. 9. Schematic $(x/y, T)$-phase diagram of $Li_{1-x}Zn_x(V_{1-y}Ti_y)_2O_4$ for $0 \le x \le 0.3$ and $0 \le y \le 0.3$. The abbreviations denote the following states: PM/M, paramagnetic metallic; I, insulating; SG/M spin-glass metallic; SG/I spin-glass insulating; CG, short-range magnetic ordering.

Fujiwara *et al.* [11,27], Amako *et al.* [40] and by Muhtar *et al.* [41]. A schematic phase diagram is shown in Figure 9. The characteristic temperatures have been taken from the susceptibility anomalies found in this work and by Ueda *et al.* [19]. As demonstrated in Figure 9, pure LiV_2O_4 indeed remains a paramagnetic metal down to the lowest temperatures and seems to be directly located at a spin-glass QCP. The square root dependence of the heat capacity (see Fig. 7) seems to corroborate this behavior. However, we clearly have to state that the single-crystalline resistivity investigations by Urano *et al.* point toward a pure Fermi-liquid behavior, while for a spin-glass QCP a $T^{3/2}$ behavior is expected [2].

On Zn doping the freezing temperature increases almost linearly with $T_f = 44 \times x$, reaching values close to 14 K for $x = 0.3$. It seems that close to the metal-insulator phase boundary this linear increase stops and for higher Zn doping, within the insulating phase, the freezing temperature almost remains constant [11,19]. At this phase boundary for the Zn doped samples the NMR, heat-capacity and susceptibility anomalies roughly coincide within experimental uncertainties, having in mind that the freezing temperature not only depend on temperature and concentration, but also on the external magnetic field and on the time scale (frequency) of the measurements. Ti doping at the B sites also removes the full and ideal geometrical frustration. But in this case the freezing temperatures only weakly depend on concentration and remain rather low. However, in this Ti concentration regime a second phase follows the low-temperature spin-glass state and precedes the purely paramagnetic phase. This precursor phase may indicate the appearance of short-range ordered clusters, before spin-glass behavior evolves throughout the bulk sample at somewhat lower

temperatures. It is important to note that this first phase boundary close to 10 K clearly appears in the temperature dependence of the spin-lattice relaxation rate as a broad anomaly, but reveals only a weak splitting in the FC and ZFC branches in the susceptibility measurements. In the NMR experiments the second transition is almost invisible, while in the susceptibility here the cusp shaped anomalies show up followed by a strong splitting of FC and ZFC curves.

In conclusion, we have presented susceptibility, microwave resistivity, magnetic resonance and heat-capacity results for a series of Zn and Ti doped LiV_2O_4 samples. For all doping levels the paramagnetic Curie-Weiss temperatures remain negative, and their values scatter around an average value close to that for the pure compound ($\Theta \approx -36$ K), which also is similar to that of earlier reports [5,22]. From these experiments, the transition from a system dominated by antiferromagnetic fluctuations at low temperatures to an almost ferromagnetic metal, as have been observed in neutron scattering experiments, can not be reconciled [12]. The inverse susceptibilities reveal antiferromagnetic interactions for $T > 100$ K and exhibit significant deviations from a simple CW-like behavior for $T < 50$ K. The paramagnetic moments are not too far from a value that can be derived for a system with one localized electron ($S = 1/2$) per vanadium site, although we agree that this localized spin picture certainly is heavily oversimplified. The samples are EPR silent, but the defect susceptibility strongly is coupled to the spin fluctuations of the bulk sample. From the temperature dependence of the spin-lattice relaxation rate we found an almost critical dynamics in the Zn doped compounds close to the freezing temperatures, while in the Ti doped samples only broad anomalies were observed in $1/T_1(T)$. In LiV_2O_4 the temperature dependence of the heat capacity can at best be described using a NFL model, appropriate for a system close to a spin-glass QCP. However, this behavior is not in accord with the results from electrical resistivity measurements which imply a pure Fermi liquid [2]. The spin-glass transitions in the doped compounds are indicated as cusp-shaped anomalies close to the freezing temperatures. Only a small fraction of the total vanadium entropy is lost at the spin-glass transition. In agreement with the results of Urano *et al.* [2], $\Delta S(T)$ is rapidly quenched around T_g. For LiV_2O_4 the spin-glass transition is completely suppressed and the quenching of the residual entropy continues gradually with $T \to 0$, resulting in a large increase of the Sommerfeld coefficient. It has been speculated that probably charge order and orbital order may play a role. From the single crystal resistivity [2] charge order certainly can be ruled out and the temperature dependence of the magnetic entropy reveals no significant contributions from the orbital degrees of freedom.

References

1. D.B. Rogers, J.L. Gillson, T.E. Gier, Solid State Commun. **5**, 263 (1967).
2. C. Urano, M. Nohara, S. Kondo, F. Sakai, H. Takagi, T. Shiraki, T. Okubo, Phys. Rev. Lett. **85**, 1052 (2000).
3. J.C. Johnston, J. Low Temp. Phys. **25**, 145 (1976); R.W. McCallum, D.C. Johnston, C.A. Luengo, M.B. Maple, J. Low Temp. Phys. **25**, 177 (1976).
4. E.J.W. Verwey, Nature **144**, 327 (1939); E.J.W. Verwey, Physica **8**, 979 (1941).
5. S. Kondo, D.C. Johnston, C.A. Swenson, F. Borsa, A.V. Mahajan, L.L. Miller, T. Gu, A.I. Goldman, M.B. Maple, D.A. Gajewski, E.J. Freeman, N.R. Dilley, R.P. Dickey, J. Merrin, K. Kojima, G.M. Luke, Y.J. Uemura, O. Chmaissem, J.D. Jorgensen, Phys. Rev. Lett. **78**, 3729 (1997).
6. O. Chmaissem, J.D. Jorgensen, S. Kondo, D.C. Johnston, Phys. Rev. Lett. **79**, 4866 (1997).
7. A. Krimmel, A. Loidl, M. Klemm, S. Horn, H. Schober, Phys. Rev. Lett. **82**, 2919 (1999).
8. V.I. Anisimov, M.A. Korotin, M. Zölfl, T. Pruschke, K. Le Hur, T.M. Rice, Phys. Rev. Lett. **83**, 364 (1999).
9. C.M. Varma, Phys. Rev. B **60**, R6973 (1999).
10. N. Fujiwara, Y. Ueda, H. Yasuoka, Physica B **237 & 238**, 59 (1997).
11. N. Fujiwara, H. Yasuoka, Y. Ueda, Phys. Rev. B **59**, 6294 (1999).
12. A. Krimmel, A. Loidl, M. Klemm, S. Horn, H. Schober, Phys. Rev. B **61**, 12578 (2000); A. Krimmel, A. Loidl, M. Klemm, S. Horn, H. Schober, Physica B **276 & 278**, 766 (2000).
13. J.S. Gardner, S.R. Dunsiger, B.D. Gaulin, M.J.P. Gingras, J.E. Greedan, R.F. Kiefl, M.D. Lumsden, W.A. MacFarlane, N.P. Raju, J.E. Sonier, I. Swainson, Z. Tun, Phys. Rev. Lett. **82**, 1012 (1999).
14. A.P. Ramirez, A. Hayashi, R.J. Cava, R. Siddhartan, B.S. Shashy, Nature **399**, 333 (1999).
15. B. Canals, C. Lacroix, Phys. Rev. B **61**, 1149 (2000); B. Canals, C. Lacroix, Phys. Rev. Lett. **80**, 2933 (1998).
16. R. Ballou, E. Leliévre-Berna, B. Fåk, Phys. Rev. Lett. **76**, 2125 (1996).
17. J. Villain, Z. Phys. B **33**, 31 (1979).
18. Y. Yamashita, K. Ueda, Phys. Rev. Lett. **85**, 4960 (2000).
19. Y. Ueda, N. Fujiwara, H. Yasuoka, J. Phys. Soc. Jpn **66**, 778 (1997).
20. B.L. Chamberland, T.A. Hewston, Solid State Commun. **58**, 693 (1986).
21. W. Trinkl, N. Büttgen, H. Kaps, A. Loidl, M. Klemm, S. Horn, Phys. Rev. B **62**, 1793 (2000).
22. S. Kondo, D.C. Johnston, L.L. Miller, Phys. Rev. B **59**, 2609 (1999).
23. D.C. Johnston, C.A. Swenson, S. Kondo, Phys. Rev. B **59**, 2627 (1999).
24. W. Trinkl, A. Loidl, M. Klemm, S. Horn, Phys. Rev. B **62**, 8915 (2000).
25. K. Kawakami, Y. Sakai, N. Tsuda, J. Phys. Soc. Jpn **55**, 3174 (1986).
26. M. Lohmann, J. Hemberger, M. Nicklas, H.A. Krug von Nidda, A. Loidl, M. Klemm, G. Obermeier, S. Horn, Physica B **259-261**, 963-964 (1999).
27. N. Fujiwara, H. Yasuoka, Y. Ueda, Phys. Rev. B **57**, 3539 (1998).
28. A.V. Mahajan, R. Sala, E. Lee, F. Borsa, S. Kondo, D.C. Johnston, Phys. Rev. B **57**, 8890 (1998).
29. H. Kaps, M. Brando, W. Trinkl, N. Büttgen, A. Loidl, E.-W. Scheidt, M. Klemm, S. Horn, J. Phys. Cond. Matt. **13**, L785 (2001).
30. N. Büttgen, H. Kaps, W. Trinkl, A. Loidl, M. Klemm, S. Horn, Can. J. Phys. **79**, 1487 (2001).
31. P. Fulde, *Electron Correlations in Molecules and Solids*, Vol. 100, Springer Series in Solid-State Science (Springer, Berlin, 1995).
32. T. Moriya, T. Takimoto, J. Phys. Soc. Jpn **64**, 960 (1995).
33. A.J. Millis, Phys. Rev. B **48**, 7183 (1993).
34. F. Steglich, P. Gegenwart, C. Geibel, R. Helfrich, P. Hellmann, M. Lang, A. Link, R. Modler, G. Sparn, N. Büttgen, A. Loidl, Physica B **223 & 224**, 1 (1996).
35. A.M. Sengupta, A. Georges, Phys. Rev. B **52**, 10295 (1995); S. Sachdev, N. Read, J. Phys. Cond. Matt. **52**, 9723 (1996).
36. H.-U. Desgranges, K.D. Schotte, Phys. Lett. A **91**, 240 (1982).
37. T. Hagino, Y. Seki, S. Takayanagi, N. Wada, S. Nagata, Phys. Rev. B **49**, 6822 (1994).
38. H. Kopferman, *Nuclear Moments* (Academic, New York, 1958).
39. S. Süllow, G.J. Nieuwenhuys, A.A. Menovsky, J.A. Mydosh, S.A.M. Mentink, T.E. Mason, W.J.L. Buyers, Phys. Rev. Lett. **78**, 354 (1997).
40. Y. Amako, T. Naka, M. Onoda, H. Nagasawa, T. Erata, J. Phys. Soc. Jpn **59**, 2241 (1990).
41. Muhtar, F. Tagagi, K. Kawakami, N. Tsuda, J. Phys. Soc. Jpn **57**, 3119 (1988).